Seismic Behavior of 63kV and 132kV Substation Post Insulators with Flexible Conductors, an Experimental Approach

A.H. Khalvati[1], M. Hosseini[2], and S. Mohammadpour[3]

1. Ph.D. Candidate, Graduate Program, International Institute of Earthquake Engineering and Seismology (IIEES), Tehran, Iran, * Corresponding Author; email: ah.khalvati@iiees.ac.ir
2. Associate Professor, Structural Engineering Research Center, International Institute of Earthquake Engineering and Seismology (IIEES), Tehran, Iran
3. Graduate Student, Azad Islamic University, Tehran Science and Research Branch, Tehran, Iran

ABSTRACT

Recent Earthquakes have shown that the electrical substations are very vulnerable, and direct and indirect losses resulting from their damages are highly considerable. post insulators in high-voltage substations are usually used as support for the bus bars or flexible conductors. Due to their height, low lateral stiffness and brittle materials used for the main core of such component, they have shown very poor seismic performance. In this paper, the seismic behavior of two 63kV and 132kV PIs with flexible connections to their top is studied experimentaly. Tests samples consist of individual post insulators mounted directly on the simulator platform followed by tests of complete post insulators mounted on the lattice steel structure as the support. Insulators were subjected to two different sets of inputs, first a set of sine sweeps and the second set was earthquake simulations time histories. The results of the experiments were used to verify the numerical models for further complementary assessments. The results show that they have very high frequencies and hardly can get damaged due to resonance, but the lattice steel structure decreased the natural frequencies by almost 70%, which amplifies the acceleration by %25.

Keywords:
Substation;
Seismic behavior;
Post insulator;
Shake table test

1. Introduction

Earthquakes usually cause extensive direct and indirect losses to the built environment, and among various damages those imposed to lifeline systems are more critical. Electric power network and its complex components have a key role among all other groups of lifelines such as transportation networks, pipelines, communication networks, etc. According to vast usage of electrical energy in different industries on the one hand, and the dependence of functionality of almost all other lifelines to the electric system on the other, saving the flow of the electric energy during and after an earthquake could prevent extensive direct and indirect losses. The losses include physical vulnerability and severe damages of electric equipment which are very expensive, or business interruption losses due to the electricity outage. This is particularly important in the aftermath of big earthquakes, when all lifelines should be operational, and even present extra services, for successful response activities.

Substations are among the most important parts in electric power networks, and play a vital role in stability, controllability and serviceability of electric energy, yet the experiences gained from the past earthquakes have shown that they are very vulnerable and the direct and indirect losses resulting from their damages are sometimes really considerable. This is due to using of brittle materials such as porcelains, using massive elements with a non-proper distribution of mass in height of the equipment, interaction of adjacent equipment, rigid connections, poor anchorage, insufficient lateral stiffness and strength and so on. Although several studies have been done with regard to seismic risk evaluation and mitigation of electric power systems, very few cases have discussed specifically the substations.

Hwang and Chou [1] have evaluated the seismic performance of an electric substation using event tree / fault tree technique. They have established event trees / fault trees to delineate interrelationships of the equipment. Using the fragility data of each component and the chosen technique, they have determined the probabilities that the substation, as a whole, fails at various levels of ground shaking, and have displayed the results as the substation fragility curves. Furthermore, in their study, the most critical and vulnerable component in the substation can be identified.

Anagnos [2] has developed a database that documents the performance of substation equipment in twelve California earthquakes. The purpose of the database is to provide a basis for developing or improving equipment vulnerability functions. Data have been summarized by earthquake, site, and equipment type. Probabilities of failure are calculated by dividing the number of damaged items by the total number of items of that type at the site. Using peak ground accelerations as the ground motion parameter, failure probabilities have been compared with opinion-based fragility curves for a few selected equipment classes. The comparisons have indicated that some of the existing fragility curves provide reasonable matches to the data, and others should be modified to better reflect the data.

Howard and his colleagues have presented a seismic fragility analysis of equipment and structures in an electric substation using an analytical approach [3]. Andrew Whittaker et al [4] have evaluated the seismic performance of high voltage substation disconnect switches through shake table tests.

Several studies regarding the seismic behavior of substations have been performed in *PEER* at Berkeley. Amir Gilani and his colleagues have studied the 196*kV* [5], 230*kV* [6] and 550*kV* [7] porcelain transformer bushings, and Takhirov and his colleagues have performed the seismic qualification and fragility testing of 550*kV* line break disconnect switches [8].

As it is seen, none of the studies mentioned above have focused on the post insulators as common equipment in substations. Therefore, in this paper, the main goal is to study the seismic behavior of post insulators and the dynamic characteristics of these elements by the means of shake table tests. The data gained from the tests were used to verify the numerical model. These models are used to evaluate the seismic performance of the elements.

In the following sections of the paper, at first, a brief description is presented about post insulators. Then the test procedure is described, next the numerical Finite Element (*FE*) modeling and its verification is explained, and finally, the results of the experiment and *FE* analysis are discussed.

2. Post Insulators in Substations and Their Vulnerability

The electric power networks usually consist of three basic parts:
1) Generation (i.e. power plants);
2) Transmission (i.e. transmission lines and substations between the cities having high voltages);
3) Distribution (i.e. distribution lines and substations in cities which have low voltages).

All of these components are vulnerable to earthquakes, which may result in significant disruption of power supply. Among these facilities, substation has a critical situation. An electrical substation is a facility that serves as a source of energy supply for the local area and has the main following functions:
❖ Changing the voltage level;
❖ Providing network operation safety by eliminating the lightning and surges;
❖ Providing power line control by means of measuring instruments.

Substations consist of different equipments the most important of which are:
❖ Power Transformers (*TR*);
❖ Current Transformers (*CT*);
❖ Voltage Transformers (*CVT*);
❖ Circuit Breakers (*CB*);
❖ Disconnect Switches (*DS*);
❖ Post Insulators (*PI*);
❖ Lightning and Surge Arresters (*LA*)

These equipments are usually in the switch yard. The control panels and the battery room are located in the Control Building which is near the yard. These substations are classified according to their voltage. The high-voltage substations are 400*kV* and 230*kV* ones. The above-mentioned equipments are shown in Figure (1), from left to right after the guyed tower the equipments are *LA, CVT, DS, CB, CT, PI* and *TR* respectively.
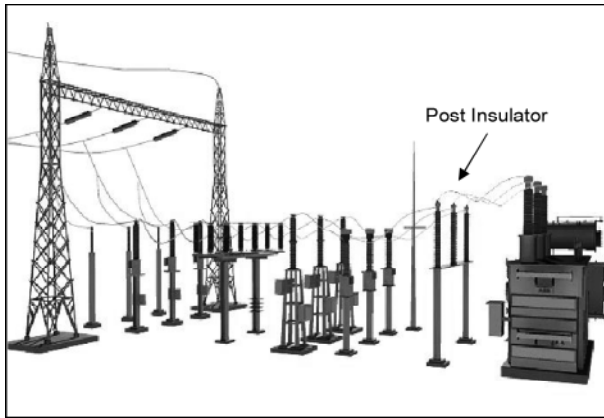
Figure 1. Typical substation configuration.

Figure 2. Post Insulators mounted on a lattice structure.

The recent earthquakes have proved that sub-stations are very vulnerable, even to moderate earthquakes. There are some obvious reasons for the observed such as [9-10]:

❖ Use of brittle materials as the main part of several equipments;

❖ Inadequate anchorage to the base;

❖ Insufficient lateral stiffness and strength;

❖ Low redundancies;

❖ Low level of damping;

❖ Interaction between adjacent equipments;

❖ Interaction between the equipment and its contents;

❖ Having heavy mass;

❖ Improper mass distribution at the height of some equipments;

❖ Poor installation and maintenance besides their remarkable ages in some cases.

It can be seen that most of the imperfections and shortcomings mentioned above can be removed and fixed with an easy attempt. However, as long as these remedies and their implementation have not been studied, the substations are considered high vulnerable and therefore, evaluation of their seismic vulnerability is of great importance.

Post insulators are widely used in substations and are commonly used as a support for the rigid aluminum bus bars or flexible conductors in order to maintain the specified height for the conductors connected to adjacent equipments. In this study, the post insulators with flexible conductors connected to the top flange are evaluated, also the slack of the connected cables to the top is assumed to be enough in order to eliminate any possible interactions between adjacent equipments, see Figure (2).
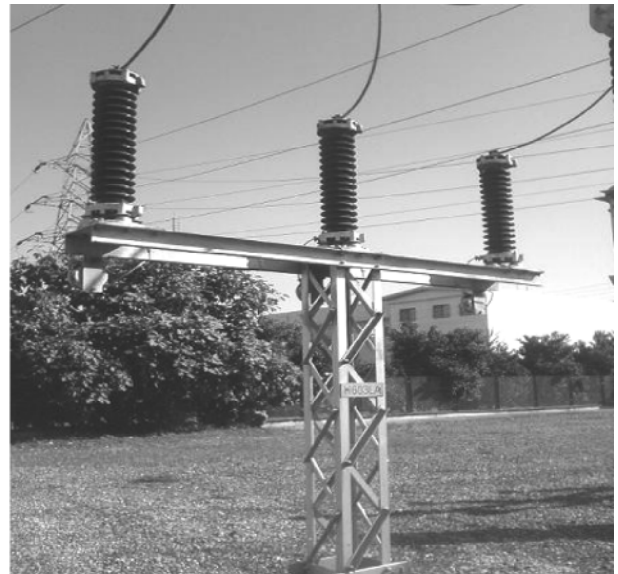
PI's usually consist of a solid porcelain core with a small diameter in similar parts that are connected to each other by cast iron flanges. According to their voltage, this may lead to a large height for the *PI* and when they become tall, their lateral stiffness decreases significantly. Also, according to the weakness and brittleness of the used ceramics they will experience sudden cracks and damages.

3. Test Specimens Characteristics

In the test procedure, two post insulator specimens $63kV$ and $132kV$ were taken, the specimens were provided by an Iranian manufacturer which is the main supplier of the substations in the country, see Figures (3) and (4).

The $63kV$ post insulator weighs $42kg$ and the $132kV$ specimen weighs $100kg$. The dimensions of these two specimens are given in Table (1).

Figure (5) illustrates the dimensions of the $63kV$ and $132kV$ specimens.

Table 1. Dimensions of the test specimens.

Dimension (mm)	63kV	13kV
Total Height	770	1500
Ceramic Part Height	610	1320
End Flange Height	80	90
Core Diameter	130	135
Total Diameter	260	260
Flange Diameter	160	260

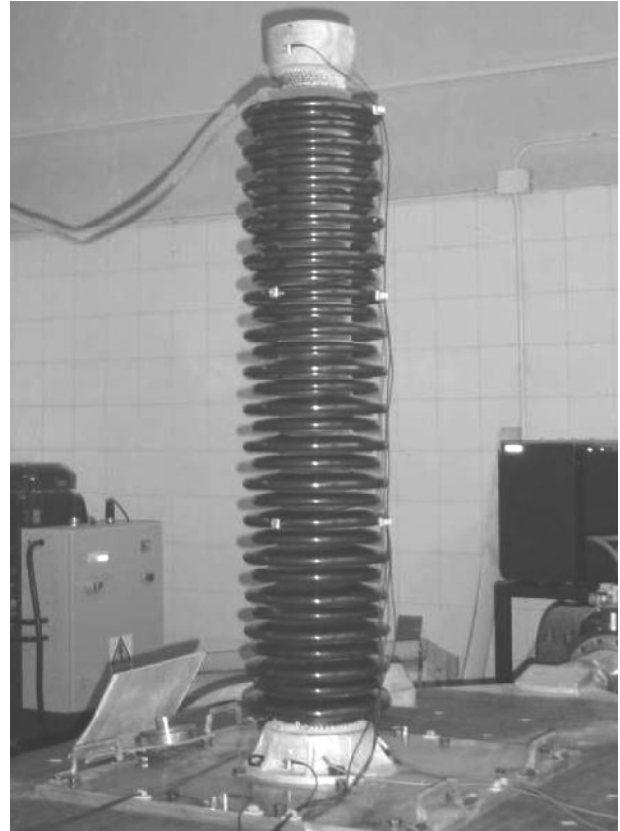**Figure 3.** 63kV Post Insulator specimen.

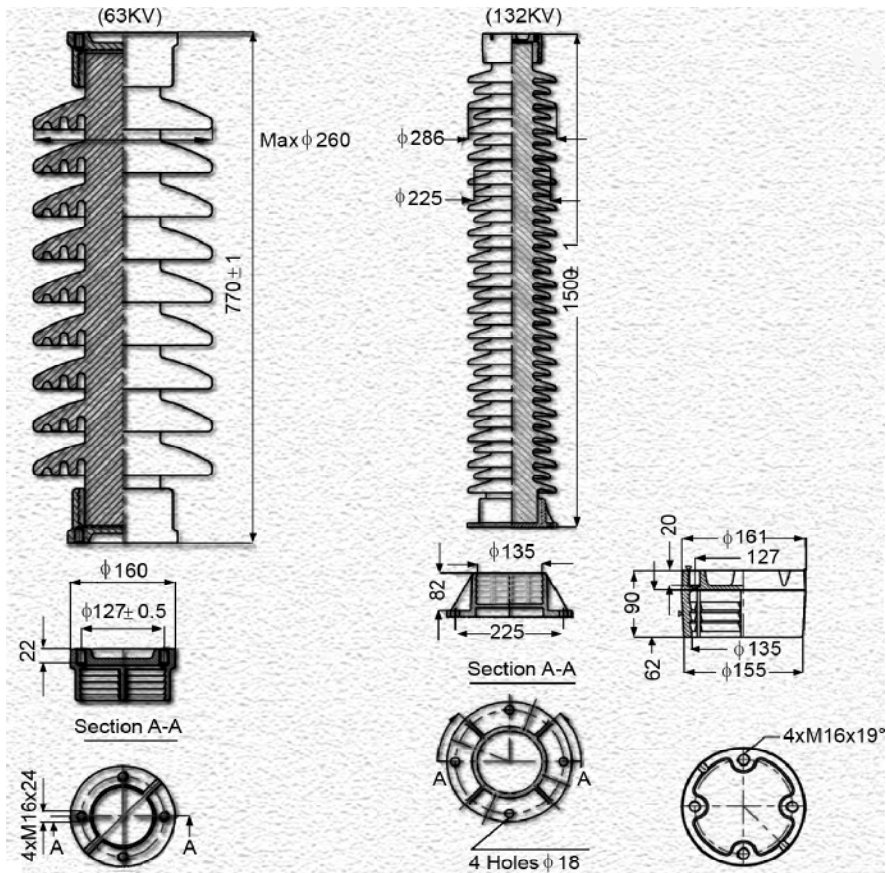**Figure 4.** 132kV Post Insulator specimen.

Figure 5. Dimensions of the 63kV and 132kV specimens.

4. Shake Table Test Setup

The shake table tests were performed in two different stages. At first, the Post insulators were mounted on the table and were shaken separately. In order to mount the specimens on the shake table, a solid $700 \times 700 \times 25 mm$ base plate made of *ST-53* steel was designed to withstand the overturning moment and to prevent any damage to the shake table surface, which its details are illustrated in Figure (6).

Post insulators are commonly mounted on a lattice steel structure. In order to simulate the actual conditions, in the second part of the test procedure, a steel structure within the actual scale and dimensions was used as a support for the *PIs*. The height of support structure was $2.45m$ and the vertical members were made of $L60 \times 60 \times 6$ angles, while the diagonal members are made of $L40 \times 40 \times 4$ angles. The *PI's* are mounted on the top plate of the structure by four bolts. The thickness of top plate is $15mm$ and the bolts are $M16$ for the $63kV$ *PI* and $M18$ for the $132PI$. The supporting structure was then welded to the thick base plate mentioned above, see Figures (7) and (8).

The shake table facility at *IIEES* structural department is manufactured by Servotest and has a unidirectional longitudinal plus vertical movement. The dimensions of the table surface are $1200 \times 1450mm$, and the maximum movement amplitude and load capacities are $35mm$ (on each side) and $2000Kg$ respectively, see Figure (9).

According to different types of the transducers, two different data loggers were used in the test, i.e. the *HBM DMCplus* and *B&K* data loggers.
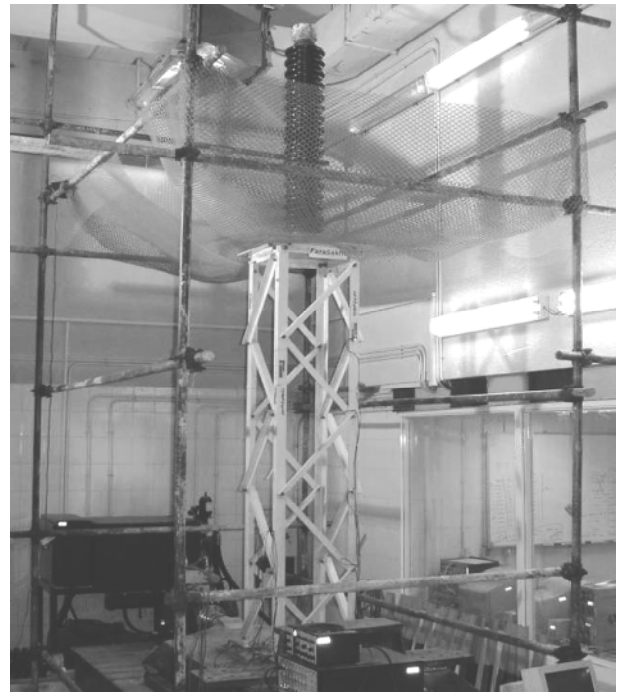
Figure 7. The 132kV PI mounted on the support structure.

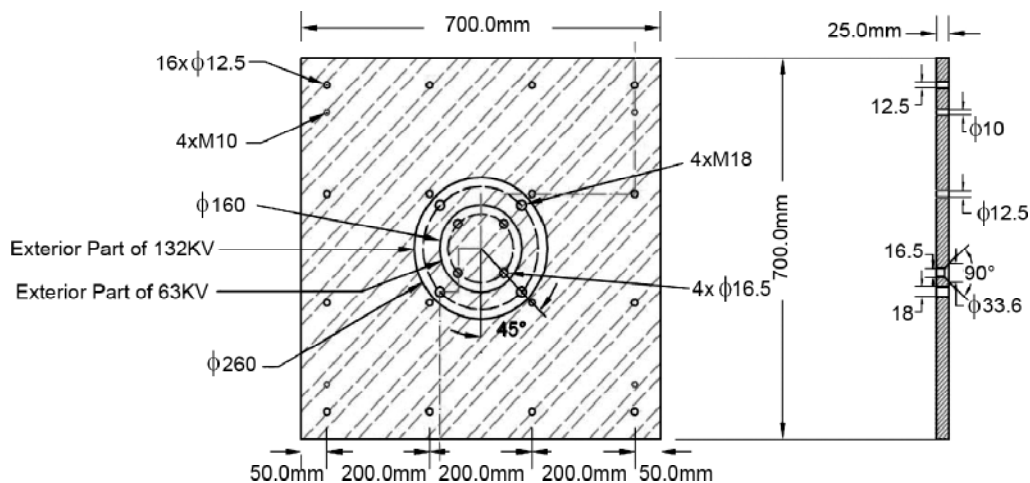**Figure 8.** The support structure prepared for test.

Figure 6. The base plate prepared for test.

Figure 9. The IIEES shake table test facilities.

One type of the transducers were *TML* strain gauge type transducers with two 2*g* and 5*g* capacities and the other type were piso-electric *B&K* high capacity (up to 100*g*) transducers. In addition to the acceleration sensors, two *FLA*6-11strain gauges were used at the bottom of the ceramic part close to the flange connection at both sides in order to record the strains' history at the most critical section of the specimens, see Figure (10).

There were four accelerometers mounted on the body of each *PI* specimen as shown in Figures (11) and (12) at the first part of the test. Two sensors were mounted at each end and two others at the 1/3 and 2/3 of the post insulators height. At the second stage of the test in which the specimens were mounted on the supporting structure, due to the lack of transducers, one of the sensors on the body of specimens was dismounted and only one sensor was mounted at the mid height of each specimen.
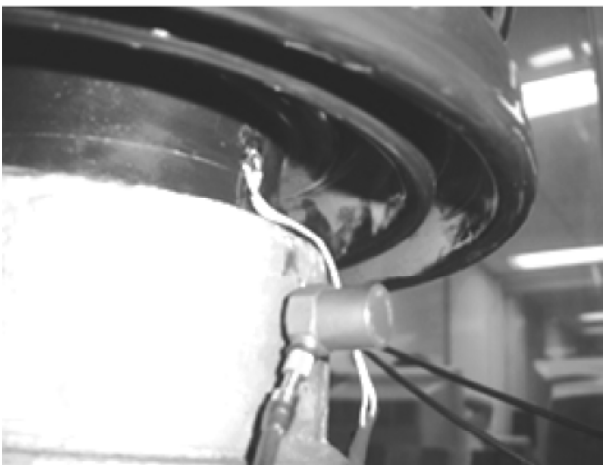

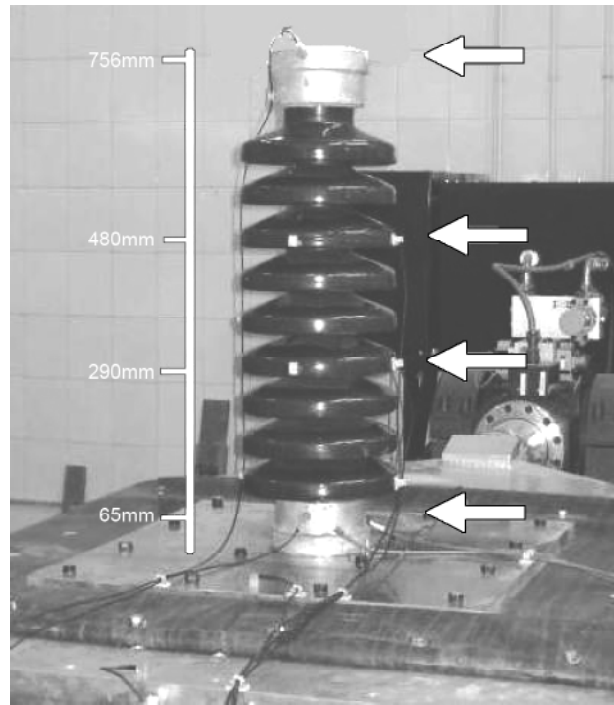**Figure 10.** The strain gauge and B&K transducers.

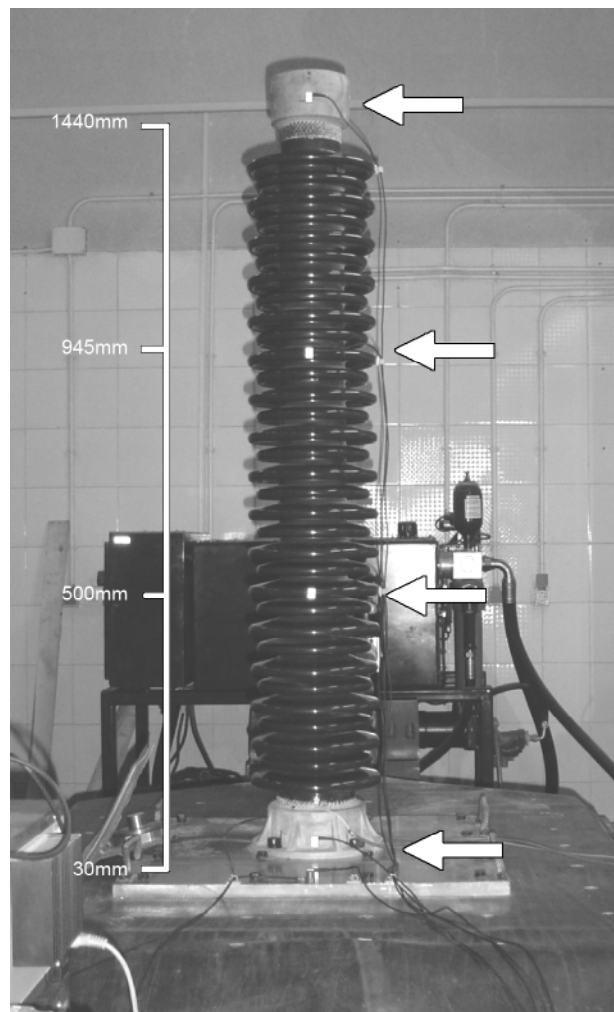**Figure 11.** The position of transducers on the 63kV specimen.

Figure 12. The position of transducers on the 132kV specimen.

In order to achieve the table accelerations, a transducer was mounted on the rigid base plate on the shaking table as shown in Figure (13), though this data could be taken as the input motions of the test.
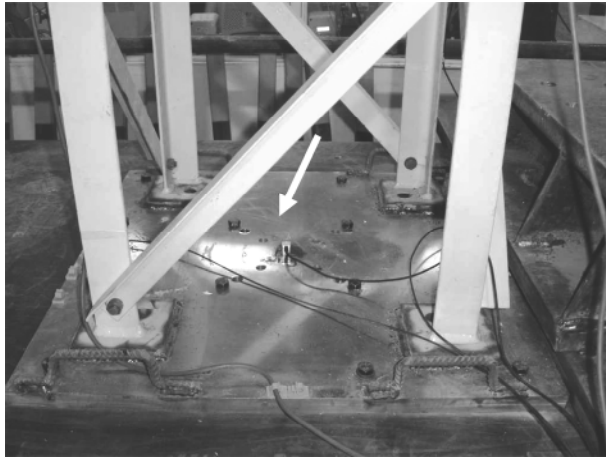

Figure 13. The position of transducer on the base plate.

The supporting structure was also tested in two stages. In the first part of the test, the lattice structure was shaken alone, and the data were taken to study this structure. In this part, there were eight transducers mounted on the structure as shown in Figure (14). Two sensors at each end and four other transducers at almost four equally divided sections on the height. As shown in Figure (15), three transducers were mounted on the top plate of the structure in vertical directions in order to record any probable torsions of the structure during the test. At the second stage of the test, the specimens were mounted on the top plate of the structure and the sensors on the height of the structure were dismounted and only one sensor was fixed at the mid height of the structure.

5. Test Procedure, Input Motions and Test Results

The input motions of the test consist of two different parts. At first, the sine sweep frequency search test was performed in order to derive the natural frequency of the test specimens. The sine sweeps were produced according to *IEEE* 693-2005 [11] recommendations. Some important notes are as below:

1) A sine sweep frequency search shall be conducted at a rate not greater than one octave per minute in the range for which the equipment has resonant frequencies but at least from 1*Hz*.
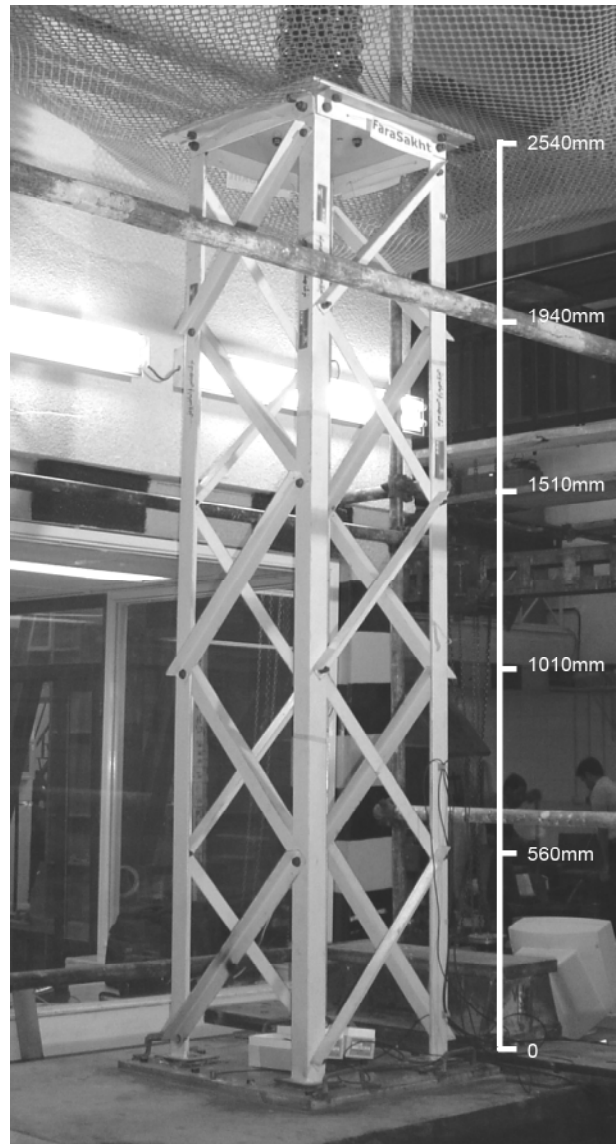

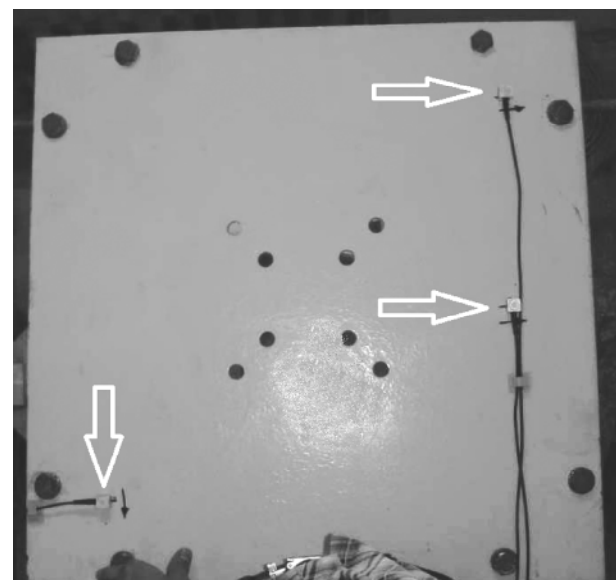**Figure 14.** The position of transducers on the lattice structure.

Figure 15. The position of transducers on the top plate.

2) The amplitude shall be no less than 0.05*g*. It is suggested that amplitude of 0.1*g* be used.

3) No resonant frequency search in the vertical axis is required.

There were some limitations to the test facility which the important ones are:

1) The maximum displacement of the table is 30*mm*.

2) At low frequencies, the maximum applicable acceleration could not exceed 1*g*.

3) The shake table input is in displacement format.

According to the above limitations and *IEEE* recommendations, 11 sweeps from 1*Hz* to 151*Hz* were produced. These sine sweeps apply the amplitude variation versus time, and the acceleration during each sweep is constant. Full descriptions of sine sweeps are given in Table (2). Figure (16) illustrates the first sweep diagram as an example.
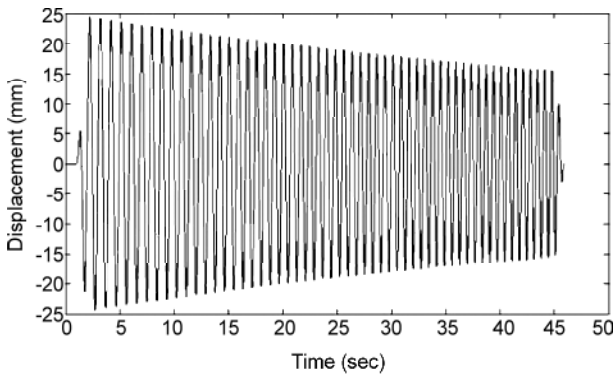

Figure 16. Input displacement history of sweep 1.

After the sine sweep tests, a set of ground motions were applied to the specimens to observe the seismic behavior of the test specimens under earthquake simulation. According to the displacement limitations of the shake table, three input ground motions were scaled down. The ground motions' specifications are presented in Table (3). The first record is the *IEEE* spectrum compatible time history ground motion which is provided by the *IEEE* 693.

In order to validate the acceleration transducers, at first, the transducers were mounted on the table individually, and the recorded data were compared with the table input motions. As shown in Figure (17), the blue plot is the input and the red plot is the recorded data by the transducers, as it is seen, they match very well. As mentioned before, each specimen was tested in two stages. At first, they were tested individually, and then the test was repeated after mounting the specimen on the lattice steel structure support. The eleven prepared sweeps and five earthquake simulations were applied to the specimens respectively. After each test, the specimens were inspected precisely in order to evolve any probable cracks and minor damages.

According to light weight of the specimens in comparison to 230*kV* and 400*kV* post insulators and low frequency content of ground motions applied, no cracks and damages were observed. The main results of the tests are recorded acceleration time

Table 2. Input sine sweeps characteristics.

Sweep	Start Frequency	End Frequency	Acceleration (g)	Maximum Amplitude (mm)	Duration (sec)
Sweep 1	1	1.6	0.1	24.85	45
Sweep 2	1.5	2.5	0.1	11.04	45
Sweep 3	2.4	4	0.1	4.31	45
Sweep 4	3.9	6.5	0.1	1.63	45
Sweep 5	6	10	0.25	1.72	45
Sweep 6	9	15	0.25	0.77	45
Sweep 7	14	23.5	1.0	1.27	45
Sweep 8	22	36	1.0	0.51	45
Sweep 9	34	57	2.0	0.42	45
Sweep 10	55	92	4.0	0.33	45
Sweep 11	90	151	4.0	0.12	45

Table 3. Input ground motions characteristics.

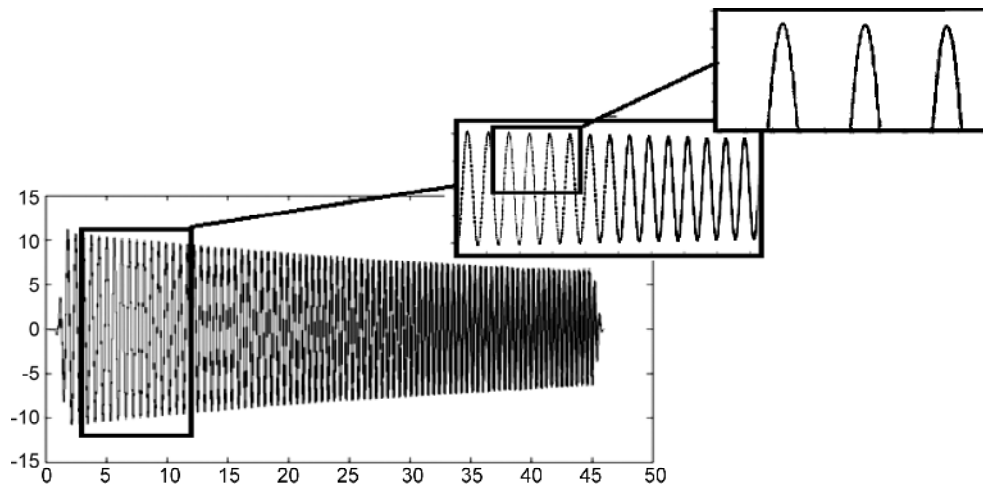| Name	PGA (g)	PGD (cm)	Duration (sec)	Scale Factor
IEEE Compatible	0.0604	2.98	39.99	0.065
Imperial Valley	0.0716	2.99	39.99	0.23
Tabas	0.133	2.99	23.82	0.39
Northridge	0.562	2.91	39.98	1.0
Coalinga	0.605	2.32	39.99	1.0

Figure 17. Recorded data and the input motion comparison.

histories at the points where the sensors were mounted. By computing the *FFT* of the response of the specimens to each sweep the natural frequency of the *PI* is derived using Peak Picking Method (*PPM*).

Peak Picking Method is based on the fact that absolute value of the Fourier transform of a structure response will usually have peaks at the modal frequencies and perhaps also at the input frequencies. The plot of the absolute value of the discrete Fourier transform (*DFT*) as a function of frequency which is called periodogram for the response of the top flange to sweep 1 is presented in Figure (18) as an example. As it is obvious the first mode frequency is about 70 *Hz*. The frequencies gained by the test are given in Table (4).

Table 4. Post Insulators 1st mode frequencies obtained by sine sweep test.

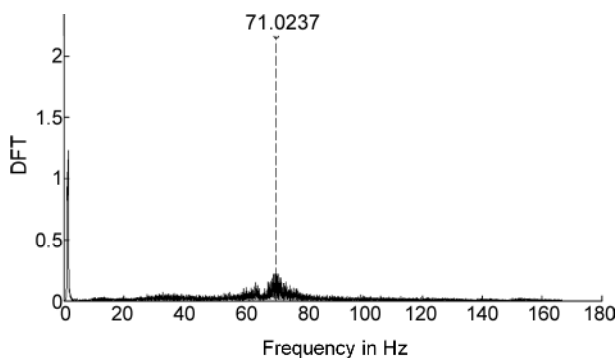| Specimen	Without Structure	Mounted on Structure
63 kV	70 Hz	19 Hz
132 kV	28 Hz	9 Hz

Figure 18. Response of the top flange to the first sweep.

According to very high values of the frequencies of higher modes, they could not have been evolved by the test and were calculated by the *FE* modeling and modal analysis of the numerical model which the results are presented in the next section of the paper. As it is seen in Table (4), the lattice support structure has a noticeable effect on reducing the natural frequency of the Post Insulators, in some cases, the reduction is almost 75%. This will lead to higher responses and seismic demands of the equipments.

6. Finite Element (FE) Modeling

Using reliable *FE* software, the analytical models of the post insulators were prepared. The model consists of four parts:

- ❖ Part 1: The bottom flange which is made of cast iron and is modeled by solid element, Figure (19);
- ❖ Part 2: The main core which is made of porcelain and is modeled by solid element, Figure (20);
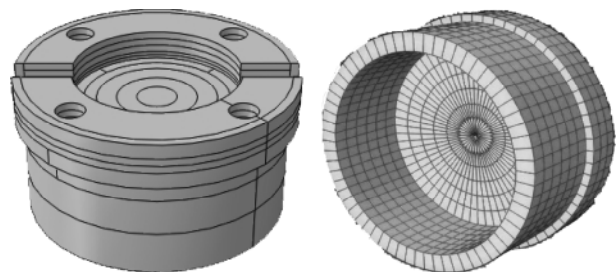- ❖ Part 3: The top flange of the *PI* which is made of cast iron and is modeled by solid element, Figure (19);

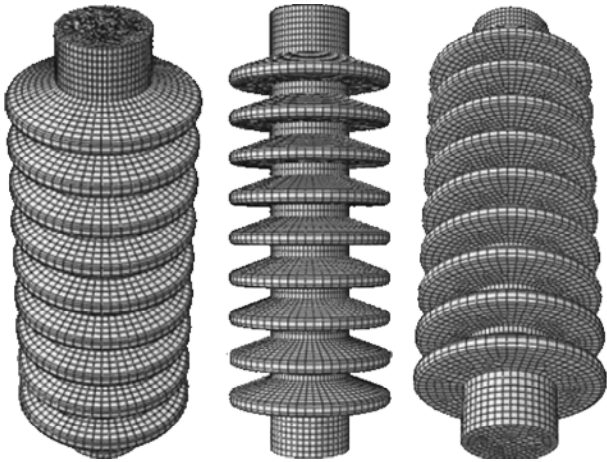**Figure 19.** The top and bottom flange of the model.

Figure 20. The porcelain part of the model.

❖ Part 4: The steel structure which is modeled by wire frame elements and hinge connections, Figure (21). The lattice steel structure model.

The mechanical properties of the materials assumed in the modeling of the specimens are presented in Table (5). These properties are based on the *IEEE* 693-2005 [11] recommendations. The damping of these equipments is very low and rarely increases 2%, so according to *IEEE* recommendations the damping ratio is assumed to be 2%.
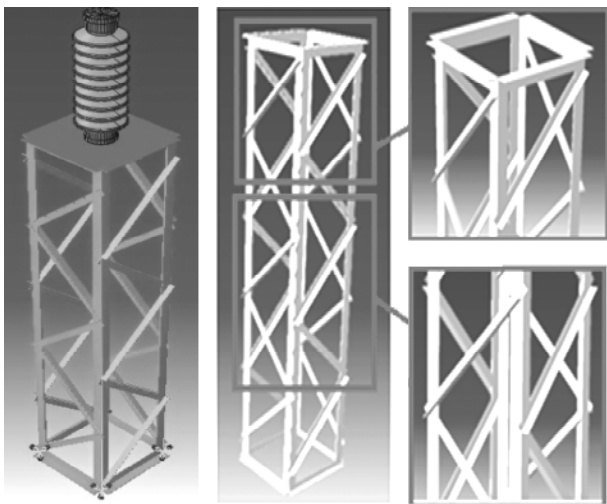

Figure 21. The lattice steel structure model.

Table 5. The material properties assumed in finite element modeling.

Material	Young's Modulus (N/mm²)	Poisson's Ratio
Porcelain	70000	0.24
Steel	210000	0.3
Cast Iron	157000	0.3

In order to verify the analytical model with the experimental results, two main criteria were chosen. The first criterion was the natural frequencies of the Post Insulators, and the second was the acceleration response of the test specimens compared to the analytical model to the same input. The analytical model was modified in order to match these two criteria.

The natural frequencies finally derived from the modified analytical model are given in Table (6), and they are also compared to the frequencies evolved from the sine sweep frequency search test. As it is obvious, the results are close together and the model could be reliable enough for further studies.

Table 6. Post insulators 1ˢᵗ mode frequencies derived from analytical model and sine sweep test.

Specimen	Experimental		Analytical	
	Without Structure	Mounted on Structure	Without Structure	Mounted on Structure
63kV	70Hz	19Hz	68.8	19.8
132 kV	28Hz	9Hz	29.4	8.1

In addition to frequency matching, as noted above, the responses were also compared. As shown in Figure (22) for an example, the recorded acceleration time history of the top flange of 63kV specimen from the sine sweep test is compared to the numerical model response at the same node and with the same input. It has to be noted that the input of the numerical model is the recorded acceleration of the sensor on the base plate as shown in Figure (23). As it is seen, there is a high-frequency noise recorded by the transducers during the test due to the vibration of the shake table facilities (blue plot), but the whole pattern matching is satisfying.

In order to verify the analytical model, many sensitivity analyses were performed, and the effect of changing different material properties as well as modelling assumptions and elements adjustments were studied. As shown in Figures (24) and (25), the effect of changing the modulus of elasticity of the porcelain on the 1ˢᵗ mode natural frequency and the maximum stress of the porcelain part is negligible, so the value presented by the *IEEE* was chosen.

Another parameter that its effects on the results of the analytical model have been studied is the elements' mesh size in *FE* modeling of the specimens. As shown in Figure (26), the first mode frequency of the 63kV Post Insulator will slightly
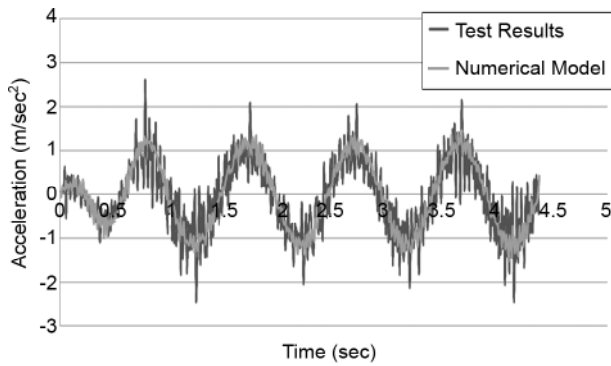
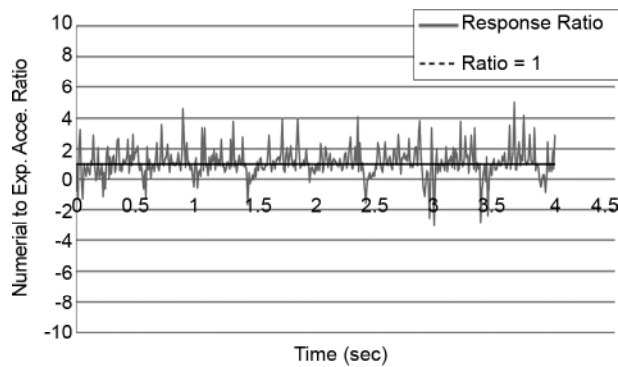**Figure 22.** Comparison of the analytical model and test specimen responses.

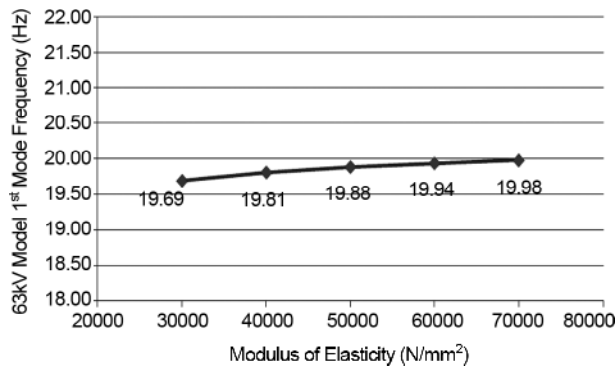**Figure 23.** Numerical to experimental acceleration ratio.

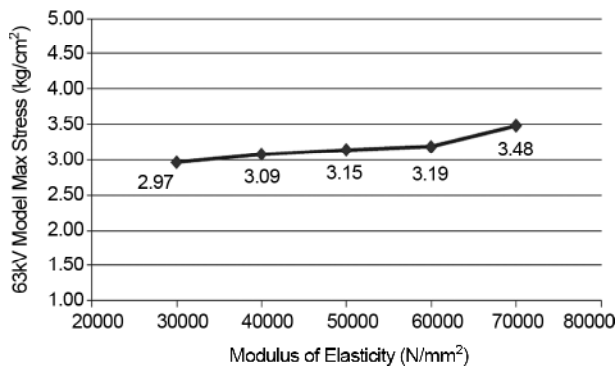**Figure 24.** The effect of modulus of elasticity on the numerical model frequency.

Figure 25. The effect of modulus of elasticity on the porcelain max stress.
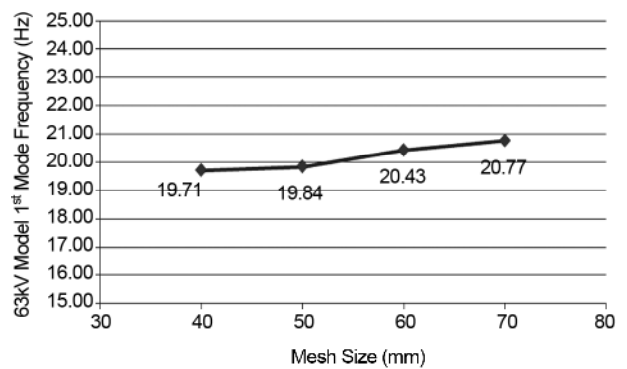

Figure 26. The effect of mesh size on the frequency of the analytical model.

change by increasing the mesh size, yet considering the time spent for time history analysis and the desired precision, the size of the elements' mesh has been chosen 50*mm*.

7. Seismic Evaluation of Insulators

After verification of the numerical model, the natural frequencies of the Post Insulators' higher modes were derived by the modal analysis, and the results are presented in Table (7). According to the symmetry of the models, the frequencies of the first two sequential modes are close together.

In order to evaluate the seismic response of the specimens, the acceleration response of the top and bottom flanges of *PI* and the base plate are plotted. Figures (27) to (29) present responses of the 63*kv* Post Insulator mounted on the structure to Sweep 1.

The base plate acceleration could be taken as input for the specimens. As it is seen, the response of the bottom flange is maximum 2.2 *m/s²* which is very close to the base plate acceleration (i.e. 2.05*m/s²*), this means the structure is rigid enough, but the top flange response of the *PI* reaches to 3.1 *m/s²* that is almost 40% more than bottom flange and 50% more than the base acceleration.

Table 7. Post Insulators higher mode frequencies derived from numerical model (Hz).

Mode	63 kV		132 kV	
	Without Structure	Mounted on Structure	Without Structure	Mounted on Structure
1	68.81	19.84	29.45	8.14
2	68.81	19.84	33.52	11.42
3	408.55	65.77	186.93	37.86
4	526.19	65.77	202.99	45.69
5	560.90	104.56	258.88	63.96

The analytical responses of the $63kv$ Post Insulator mounted on the structure derived from the dynamic analysis for sweep 1 are given below.

Based on Figures (30) and (31) the experimental accelerations at the top and bottom flanges are $2.2m/s^2$ and $1.95m/s^2$ respectively. As discussed in previous sections, see Figure (23), due to the high-frequency noise, the analytical and experimental accelerations are not identical.

Figure (32) illustrates the acceleration of the top flange of $63kV$ PI mounted directly on the base plate. The maximum acceleration is $2.5m/s^2$ that is almost 80% of the maximum acceleration of the same point when mounted on the support structure. This means that the support amplifies the acceleration by almost 1.25.
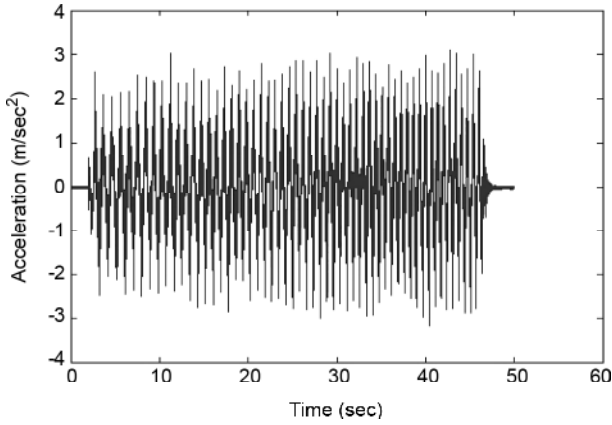

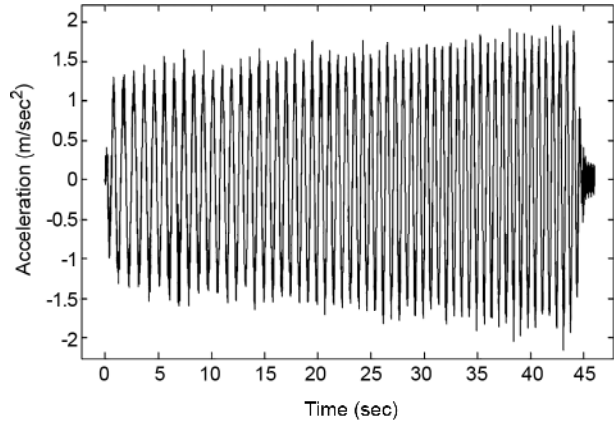**Figure 27.** Experimental top flange acceleration.
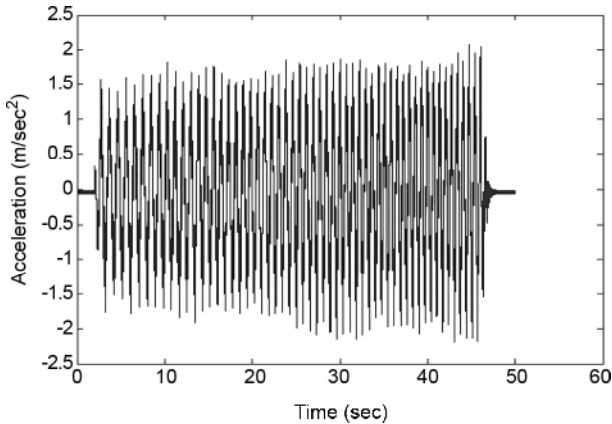

Figure 30. Analytical top flange acceleration .

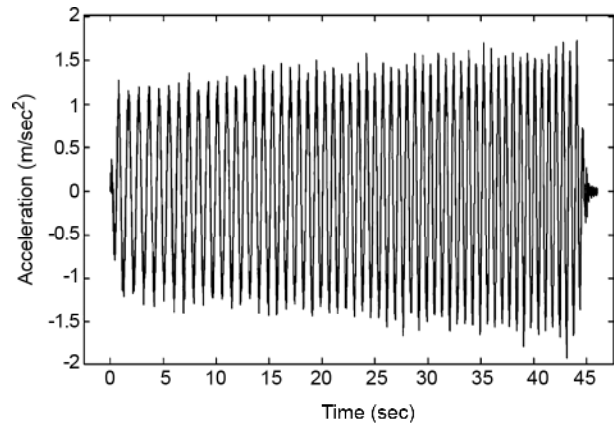**Figure 28.** Experimental bottom flange acceleration.

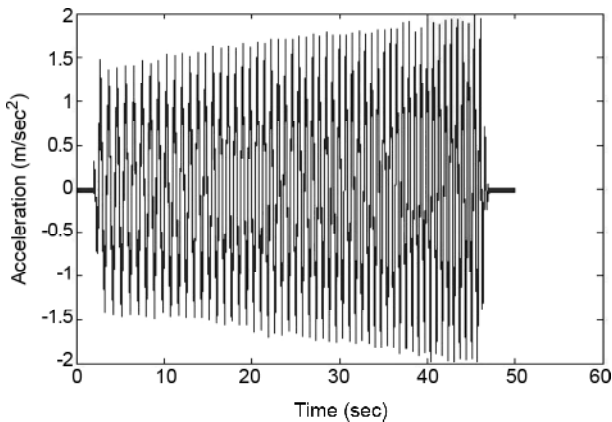**Figure 31.** Analytical bottom flange acceleration.

Figure 29. Experimental base plate acceleration.
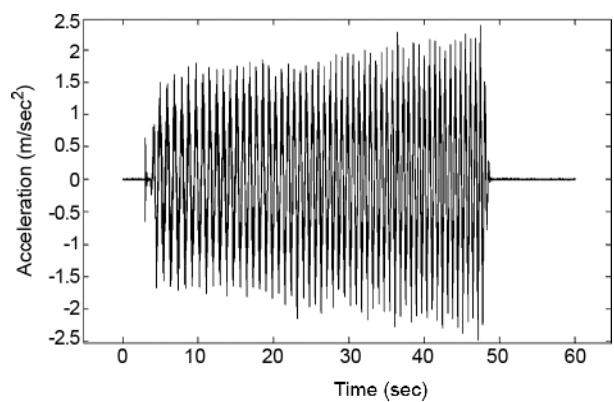

Figure 32. Experimental top flange acceleration of post insulator without the support structure.

Figure (33) illustrates the analytical acceleration of the top flange without structure. Compared to Figure (32), it could be found out the maximum experimental and analytical accelerations are very close.
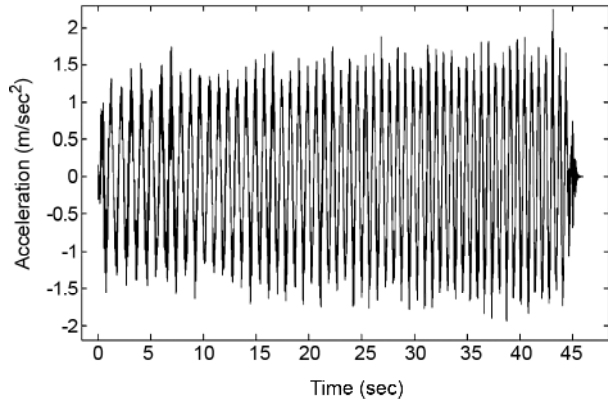

Figure 33. Analytical top flange acceleration response of post insulator without the support structure.

The Figures (34) to (36) present responses of the 63kv Post Insulator mounted on the structure to the *IEEE* proposed ground motion input.

As it is seen, the maximum response of the bottom flange is 9.6m/s^2 that is almost 41% greater than the base plate acceleration which is 6.8m/s^2, but the top flange response reaches to 13.1m/s^2 that is 92% more than base plate acceleration. This means that the amplification of the response acceleration is about 1.92.

Figure (37) illustrates the analytical top flange displacement of the 63kV PI mounted on the structure. There were no displacement sensors used during the test due to the high-frequency vibration of the specimens, so only the analytical results are presented. The maximum displacements of the top and bottom flanges are 24.69mm and 24.53mm respectively so that the relative displacement is 0.16mm. Of course, the maximum displacements will differ by different inputs.

Figures (38) and (39) illustrate the maximum experimental strains at the sensors mounted on the base of the specimens. The maximum strain at the specimen with structure is 5.02$Micro m/m$ and the specimen without structure is 4.30$Micro m/m$ which is increased by 17%.

Further studies were undertaken in order to evaluate the maximum stress which is developed at the base of the porcelain part. By performing the
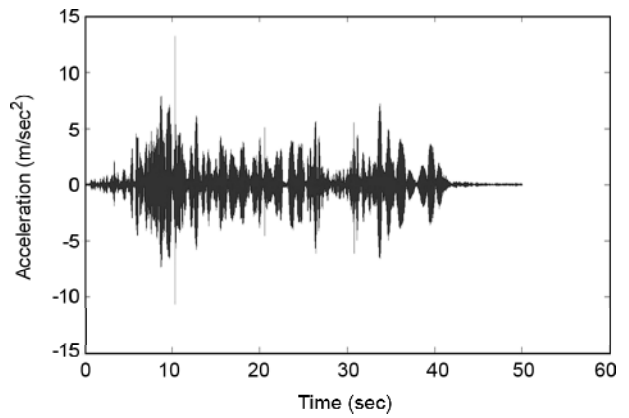

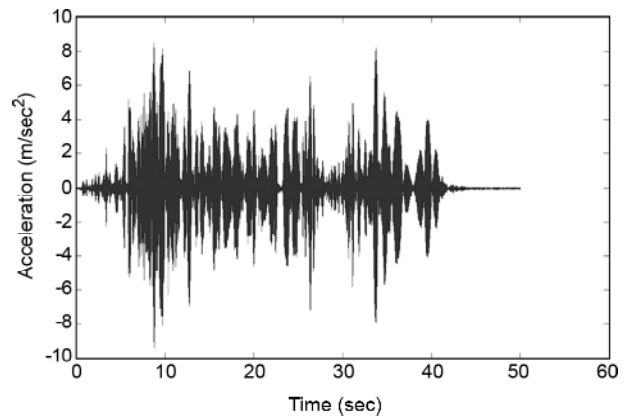**Figure 34.** Experimental top flange acceleration.

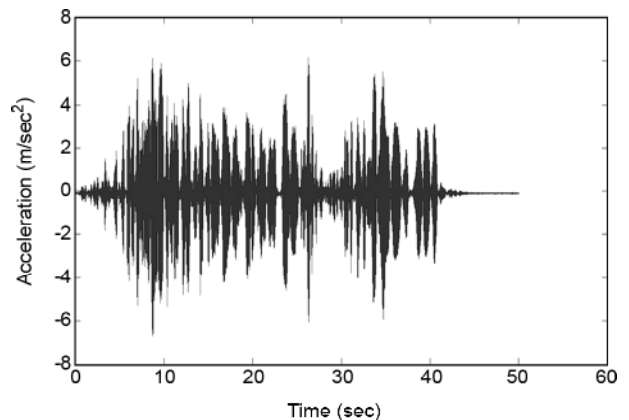**Figure 35.** Experimental bottom flange acceleration.

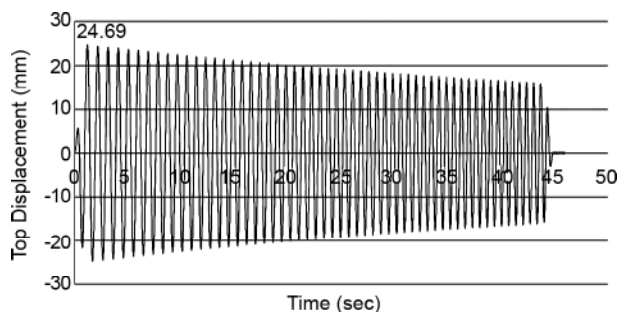**Figure 36.** Experimental base plate acceleration.

Figure 37. Analytical top flange displacement.

dynamic analysis of the numerical model the critical section of the specimen is evolved. Figure (40) illustrates the stress distribution at the base of the model and the critical section with the maximum stress at the base of the specimen is shown.

13 classes of earthquake ground motion, each group representing a *PGA* as mentioned in Table (8) were selected with suitable frequency content and dominant frequency close to that of the specimens. These records were selected from the soil types *A* and *B* in order to amplify higher frequencies. The maximum stresses are from nearly 70 dynamic analyses are given in attached table.
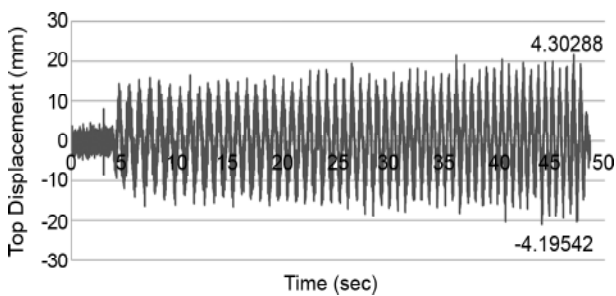

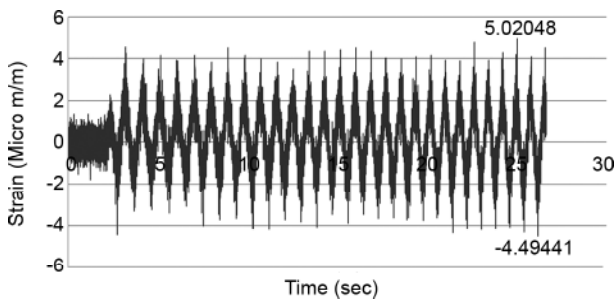**Figure 38.** Experimental strain at the base of the 63kV specimen mounted directly on the table.

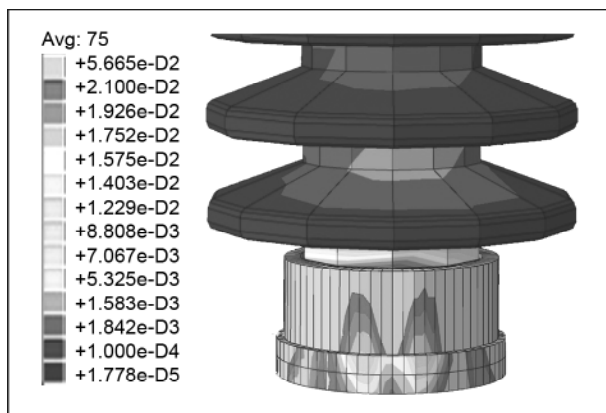**Figure 39.** Experimental strain at the base of the 63kV specimen mounted on the structure.

Figure 40. Stress Distribution at the Bottom flange from analysis.

Table (8). Input ground motions and the maximum stress gained from FE analysis of 63kV PI.

| PGA Class (g)	Event	PGA (g)	$F_{(max)}$ (Hz)	$Sa_{(max)}$ (g)	Stress (kg/cm²)
0.1g	Anza	0.081	16.8	0.3	23.10
0.1g	Coyote Lake	0.103	10	0.345	38.72
0.1g	Hollister	0.105	10	0.34	26.20
0.1g	Anza	0.11	12.5	0.485	79.57
0.1g	San Francisco	0.112	4.8	0.45	31.51
0.1g	Northridge	0.112	8.5	0.365	43.38
0.1g	Northern Calif	0.115	7.1	0.51	22.18
0.2g	Whittier Narrows	0.186	6.5	0.73	28.51
0.2g	Santa Barbara	0.203	1.9	0.55	10.30
0.2g	Loma Prieta	0.209	3	0.7	65.99
0.2g	Friuli, Italy	0.212	3	0.92	18.41
0.2g	Northridge	0.217	25	0.72	15.73
0.2g	Livermore	0.22	5.5	0.87	17.89
0.2g	Whittier Narrows	0.227	10	0.75	17.67
0.3g	San Fernando	0.283	4.1	1.32	44.40
0.3g	Northridge	0.29	3.9	1.26	32.89
0.3g	Morgan Hill	0.292	4.5	1.2	26.10
0.3g	Whittier Narrows	0.299	7.2	1.2	77.85
0.3g	Northridge	0.301	3	1.05	12.75
0.3g	Whittier Narrows	0.304	1.5	0.9	18.70
0.3g	Coyote Lake	0.316	3	1.42	17.32
0.4g	Cape Mendocino	0.385	4.1	1.1	21.11
0.4g	Whittier Narrows	0.396	5.5	1.75	61.38
0.4g	Whittier Narrows	0.4	7	1.26	33.43
0.4g	Northridge	0.401	4.5	1.5	29.84
0.4g	Loma Prieta	0.411	5	1.32	65.73
0.4g	Whittier Narrows	0.414	7	1.62	43.99
0.4g	Northridge	0.416	2	1.52	30.25
0.5g	Imperial Valley	0.485	6.5	1.16	53.22
0.5g	N. Palm Springs	0.492	5.5	1.65	66.91
0.5g	Northridge	0.493	1.5	2.8	25.23
0.5g	Westmorland	0.496	1.8	1.4	76.44
0.5g	Loma Prieta	0.512	6.2	2	60.57
0.5g	Northridge	0.514	1.9	1.45	19.50
0.5g	Northridge	0.516	4.5	1.18	66.90
0.6g	Victoria Mexico	0.587	12.8	0.85	78.14
0.6g	Northridge	0.59	1.5	2.15	27.32
0.6g	Northridge	0.593	1	1.95	25.22
0.6g	N. Palm Springs	0.594	7	1.6	48.34
0.6g	Kobe	0.599	2.6	2.33	34.35
0.6g	Imperial Valley	0.602	10	1.25	73.82
0.6g	Northridge	0.617	4	2.05	108.32
0.7g	Superstition Hills	0.682	5.5	1.9	47.67
0.7g	Kobe	0.693	2	1.8	40.22
0.7g	Kobe	0.694	2	2.5	38.79
0.7g	N. Palm Springs	0.694	5.5	2.1	49.45
0.7g	Morgan Hill	0.711	3.5	2.41	80.88
0.7g	Gazli USSR	0.718	3.9	1.85	182.50
0.7g	Landers	0.721	12.5	2.1	322.40
0.8g	Kobe	0.821	3	2.6	30.73
0.8g	Chi-Chi Taiwan	0.821	3.8	2.1	111.48
0.8g	Duzce Turkey	0.822	2.9	1.5	47.75
0.8g	Imperial Valley	0.835	25	2.8	126.00
0.8g	Tabas, Iran	0.836	4.1	3.4	85.54
0.8g	Northridge	0.838	12.5	2.9	366.152
0.8g	Coalinga	0.84	1.7	1.45	52.67
0.9g	Chi-Chi Taiwan	0.958	4	2.35	201.39
0.9g	Chi-Chi Taiwan	0.968	1	3.2	87.51
0.9g	Duzce Turkey	0.97	2.5	3.21	215.17
0.9g	Nahanni Canada	0.978	5.5	3.2	192.70
0.9g	Northridge	0.99	2.5	3.22	93.20
1.1g	Chi-Chi Taiwan	1.01	4.1	2.55	275.81
1.1g	Cape Mendocino	1.039	12.5	2.1	99.77
1.1g	Coalinga	1.083	25	1.8	77.42
1.1g	Nahanni Canada	1.096	10	2.8	206.94
1.1g	Chi-Chi Taiwan	1.157	1	3.5	60.94
1.1g	San Fernando	1.16	2.5	2.6	117.55
1.3g	San Fernando	1.226	2.5	3.1	195.12
1.3g	Northridge	1.285	6.2	3.8	170.42
1.3g	Morgan Hill	1.298	3.2	2	94.07
1.5g	Kobe	1.497	3.9	3.25	135.83
1.5g	Northridge	1.585	3	3.43	135.83
1.8g	Northridge	1.779	3	4.9	196.03
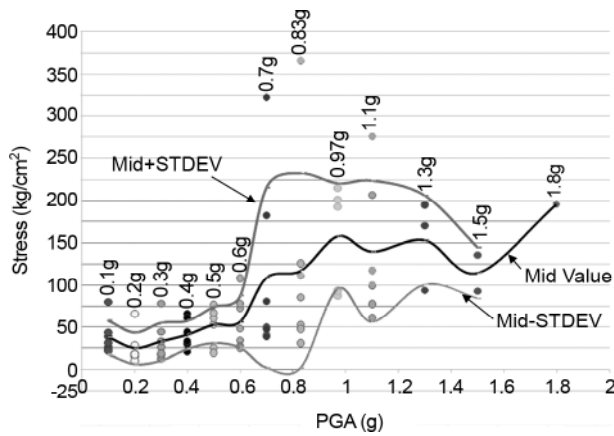
Figure 41. Max stresses at the base of 63kv specimen for different input ground motions.

The stresses for each class of *PGA* are plotted in Figure (41). The mean, mean +sigma and mean-sigma values are also plotted in the figure.

As it is seen in Figure (41), there is not a clear linear relation between the *PGA* and the maximum stress. This could be due to the fact that the natural frequency of the numerical model and the input dominant frequency are not close to each other so the resonance may not happen. This means that the *PGA* individually could not be an appropriate parameter for the seismic evaluation of these elements, and to get more acceptable results, some other characteristics of the input must be considered. This could be a subject for further studies.

In order to evaluate the effect of the support structure on the maximum stress, the *132kV PI* has been analyzed in two stages, first mounted on the structure and next individually mounted on the base. The ratios of the stresses in these two stages are given in Figure (42). As it's seen, the structure amplifies the stresses by 2.8.
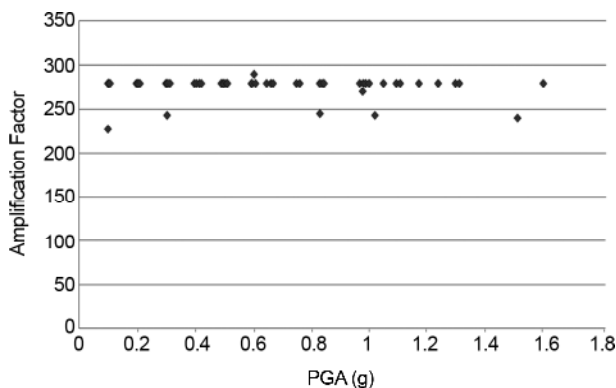

Figure 42. The amplification effect of the support structure on the 132kV PI max stress.

Due to lack of space, the full results and figures are not presented here and could be found on the main report of this study [11].

Of course, when they are mounted on the supporting structure, the frequency of the system decreases significantly, but it is still out of the range of those from ground motions.

8. Concluding Remarks

Based on the experimental and numerical studies it can be concluded that:

❖ The most considerable result of the test was that there were no significant responses from the specimens, and not any damages were observed during the earthquake simulation tests. This is because of the high-frequency content of these equipments that are much greater than that from ground motions, which is usually about 3 to $10Hz$ on one hand and their lower weights compared to $230kV$ and $400kV$ *PIs* on the other hand.

❖ Natural frequencies of insulators without supporting structure are very higher than conventional structures due to their high stiffness and low weight.

❖ The effect of supporting structure on the natural frequencies of insulators mounted on the supporting structure was evaluated. The natural frequencies decrease by almost 70%.

❖ Precision of the numerical models was verified by experimental results.

❖ Effect of the supporting structure on the amplification of the experimental top flange acceleration shows that the kind of structure used amplifies the acceleration by 1.25 compared to the *PI* without structure.

❖ Effect of the supporting structure on the amplification of the strains at the base of the specimens, shows that the type of structure used amplifies the strains by 1.17 compared to the *PI* without structure.

❖ The maximum displacements of the top and bottom flanges are $24.69mm$ and $24.53mm$, respectively, so that the relative displacement is $0.16mm$. Of course, the maximum displacements will differ by different inputs and different structures.

❖ The *PGA* individually could not be an appropriate parameter for the seismic evaluation of these elements, and to get more acceptable results,

some other characteristics of the input must be considered.

❖ Effect of the supporting structure on the amplification of the maximum stress at the base of the $132kV$ specimen shows that the kind of structure used, amplifies the maximum stress by almost 2.8 compared to the *PI* without structure. Of course, this is higher than the factor for $63kV$ *PI*.

Acknowledgments

References

1. Hwang, H. and Chou, T. (1998). "Evaluation of Seismic Performance of an Electric Substation Using Event Tree/Fault Tree Technique", *Probabilistic Engineering Mechanics*, **13**(2), 117-124.

2. Anagnos, T. (1999). "Development of an Electrical Substation Equipment Performance Database for Evaluation of Equipment Fragilities", San Jose State University.

3. Hwang, H. and Huo, J. (1998). "Seismic Fragility Analysis of Electrical Substation Equipment and Structures", *Probabilistic Engineering Mechanics*, **13**(2), 107-116.

4. Whittaker, A., Fenves, G., and Gilani, A. (2007). "Seismic Evaluation and Analysis of High-Voltage Substation Disconnect Switches", *Engineering Structures*, **29**, 3538-3549.

5. Gilani, A., Chavez, J., Fenves, G., and Whittaker, A. (1998). "Seismic Evaluation of 196kV Porcelain Transformer Bushings", PEER Report No. 1998/02, Pacific Earthquake Engineering Research Center, Berkeley, California.

6. Gilani, A., Whittaker, A., Fenves, G., and Fujisaki, E. (1999). "Seismic Evaluation of 230kV Porcelain Transformer Bushings", PEER Report No. 1999/14, Pacific Earthquake Engineering Research Center, Berkeley, California.

7. Gilani, A., Whittaker, A., Fenves, G., and Fujisaki, E. (1999). "Seismic Evaluation of 550kV Porcelain Transformer Bushings", PEER Report No. 1999/-05, Pacific Earthquake Engineering Research Center, Berkeley, California.

8. Takhirov, S., Fenves, G., and Fujisaki, E. (2004). "Seismic Qualification and Fragility Testing of Line Break 550kV Disconnect Switches", PEER Report No. 2004/08, Pacific Earthquake Engineering Research Center, Berkeley, California.

9. Khalvati, A.H. and Hosseini, M. (2008). "Seismic Performance of Electric Substations' Equipments in Iran's Recent Earthquakes", *Proc. of the 14th World Conf. on Earthquake Engineering*, China.

10. Eshghi, S. (2003). "Preliminary Report of Bam Earthquake", IIEES Report, International Institute of Earthquake Engineering and Seismology (IIEES), Tehran, Iran.

11. IEEE (2005). Recommended Practice for Seismic Design of Substations, IEEE Standards No. Std. 693-2005, The Institute of Electrical and Electronics Engineers, NY, USA.

12. Khalvati, A.H. (2012). "Experimental and Analytical Evaluation of Seismic Performance of Low-Voltage Post Insulators", PhD. Dissertation, IIEES, Tehran, Iran